Archival Report

Biological Psychiatry: GOS

Neuron-Specific Glycine Metabolism Links Transfer RNA Epitranscriptomic Regulation to Complex Behaviors

Jennifer Blaze, Viviana Dolores Evans, Jessica Abigail Feria Pliego, Petr Unichenko, Behnam Javidfar, Soeren Heissel, Hanan Alwaseem, Zachary Pennington, Denise Cai, Henrik Molina, Christian Henneberger, and Schahram Akbarian

ABSTRACT

BACKGROUND: The presence of treatment resistance in neuropsychiatric disease suggests that novel mechanism-based discoveries and therapies could benefit the field, with a viable candidate being transfer RNA (tRNA) epitranscriptomics. *Nsun2* tRNA methyltransferase depletion in mature neurons elicits changes in complex behaviors relevant for fear, anxiety, and other neuropsychiatric phenotypes. However, it remains unclear whether this is due to dysregulated tRNAs or metabolic shifts that impact the neuronal translatome by activation of stress messengers together with alterations in amino acid supply.

METHODS: To link specific molecular alterations resulting from neuronal *Nsun2* ablation to neuropsychiatric phenotypes, we used drug-induced phosphoactivation of stress response translation initiation factors together with disruption of NSUN2-regulated glycine tRNAs and cell type–specific ablation of the glycine cleavage system modeling the excessive upregulation of this amino acid in the *Nsun2*-deficient brain. Changes in extracellular glycine levels were monitored by an optical glycine Förster resonance energy transfer (FRET) sensor in the hippocampus, and behavioral phenotyping included cognition, anxiety-like behavior, and behavioral despair.

RESULTS: Increased motivated escape behaviors were specifically observed in mice with neuron-specific ablation of *Gldc*, resulting in an excess in cortical glycine levels comparable to a similar phenotype in mice after deletion of neuronal *Nsun2*. None of these phenotypes were observed in mice treated with tunicamycin for chemoactivation of integrative stress response pathways or in mice genetically engineered for decreased glycine tRNA gene dosage. In the *Nsun2*-deficient brain, dynamic glycine profiles in the hippocampal extracellular space were fully maintained at baseline and in the context of neuronal activity.

CONCLUSIONS: Alterations in neuronal glycine metabolism, resulting from targeted ablation of the glycine cleavage system or disruption of the tRNA regulome, elicit changes in complex behaviors in mice relevant for neuropsychiatric phenotypes.

https://doi.org/10.1016/j.bpsgos.2024.100432

Most current neuropsychiatric pharmacological treatments for mood and anxiety disorders target monoamine neurotransmitters, glutamate, or GABA (gamma-aminobutyric acid) receptors, but with 20% to 60% of patients still experiencing treatment resistance, novel interventions are required in the field of psychiatry (1,2). Cellular metabolism is known to affect neurological phenotypes, but direct interventions targeting specific elements of cellular metabolism in the brain are rarely utilized in treating neuropsychiatric disease. One of the few notable examples includes the ketogenic diet (3), which reduces the body and brain's reliance on glucose, thereby altering neuronal excitability, and in a recent study, ketogenic diet significantly improved psychiatric symptoms in a clinical population (3).

Leveraging neuronal metabolism as a therapeutic option for psychiatric disease is a missed opportunity given some of the emerging and surprisingly extremely effective metabolic treatments in other areas of medicine. For example, glycine and serine starvation are potential therapeutics for certain forms of cancer (4,5). Glycine metabolism is also an interesting avenue for novel brain-related therapies given that glycine levels in the brain can be modestly altered following oral administration (6,7). However, glycine absorption in the gut after oral administration is variable, and it crosses the blood-brain barrier poorly (7), but imaging studies in humans and molecular studies in rodents have confirmed that there are significant increases in glycine detected in the brain after dosing orally (6,7). Oral glycine supplementation causes a modest but statistically tractable improvement in sleep quality (8,9), schizophrenia symptoms (10,11), and depression (12). The mechanism of action remains unclear, but the glycine binding site on the NMDA receptor (13,14) has been implicated most frequently.

ISSN: 2667-1743

Cellular metabolism and amino acid levels can be altered following changes in transcriptional machinery, namely transfer RNAs (tRNAs) and their modifications, with evidence of downstream effects on brain function in mice (15–17). For example, loss of $tRNA^{Arg}$ was associated with activation of the integrated stress response (ISR), a highly conserved pathway in eukaryotes that programs the translatome in times of cellular stress to restore homeostasis (18). This model also showed an increase in glycine and serine amino acids in brain tissues, affecting synaptic transmission and thereby reducing seizure threshold (15). Furthermore, global loss of NSUN2 tRNA methyltransferase, which results in loss of tRNA cytosine methylation, is associated with altered amino acid levels and a shift in cellular metabolism (17). To this end, our previous work linked the tRNA epitranscriptome to the regulation of complex behaviors, including behavioral despair, anxiety-like behavior, and cognition (19). Specifically, neuronal loss of the tRNA methyltransferase *Nsun2* depleted tRNA cytosine methylation in the brain and selectively decreased $tRNA^{Gly}$, which harbors the most NSUN2-mediated methylation sites compared with other tRNAs (19). This was associated with approximately 150% increase in glycine amino acid in the mutant brain after neuronal *Nsun2* ablation, accompanied by increases in protein levels of glycine-serine biosynthesis enzymes (19).

The goal of the current study was to mechanistically test how and by which modality neuronal glycine metabolism alters behavioral phenotypes in multiple novel rodent models, including genetically induced upregulation of glycine via glycine decarboxylase (*Gldc*) deletion, tRNA gene-specific deletion of $tRNA^{Gly}_{TCC}$, and experimental induction of the ISR, which is tightly regulated by amino acid and tRNA levels.

METHODS AND MATERIALS

Animals

All animal work was approved by the Institutional Animal Care and Use Committee of the Icahn School of Medicine at Mount Sinai. Mice were group housed 2 to 5/cage with ad libitum access to food and water and a 12-hour light/dark cycle under constant conditions (21 ± 1° C; 60% humidity). Mice bred in-house were weaned on postnatal day 28, ear-tagged/genotyped, and housed with same-sex littermates until further testing. Mice for all experiments were 8 to 16 weeks old at testing and were age matched for each experiment.

Nsun2 Conditional Knockout Mice

CamK-Cre^{+},*Nsun2*$^{2lox/2lox}$ mice (*Nsun2* knockout [KO]) were generated as described previously (19–21), and loss of *Nsun2* messenger RNA (mRNA) and protein were validated in Blaze *et al.* (19). Age-matched *Camk2a-Cre*-, *Nsun2*$^{2lox/2lox}$, or *Nsun2*$^{2lox/-}$ were used as wild-type (WT) control mice.

GLDC Conditional KO Mice

B6N(129S4)-Gldc^{tm1c}(EUCOMM)Wtsi/LutzyJ mice were purchased from the Jackson Laboratory (strain 034928). In these mice, exon 3 of *Gldc* is flanked by loxP sites, creating a conditional-ready mutant allele. We crossed these mice with the same *Camk2a-Cre*+ line referenced above for postnatal forebrain neuronal deletion of *Gldc*.

tRNAGlyTCC-1 KO Mice

Mice with a deletion of *tRNAGlyTCC-1* were generated at the Jackson Laboratory (JAX Mice, Clinical, and Research Services) using CRISPR (clustered regularly interspaced short palindromic repeats)-Cas9 through electroporation of C57BL/6J-fertilized oocytes with *Cas9* mRNA and single-guide RNAs targeting the *tRNAGlyTCC-1* family of tRNAs. Electroporated embryos were then transferred into pseudopregnant female mice to obtain live pups. The offspring were screened for deletions within the *tRNAGlyTCC-1* family of tRNAs. Three founders were selected and crossed to WT C57BL/6J mice to produce the N1 offspring: 1) a founder with a 25–base pair deletion within *tRNAGlyTCC-1-7* and an 11–base pair deletion within *tRNAGlyTCC1-5*, 2) a founder with an 11–base pair deletion at *tRNAGlyTCC-1-1*, and 3) a founder with a 25–base pair deletion at *tRNAGlyTCC-1-7*. All 3 lines of N1 animals were further bred to obtain offspring homozygous for each *tRNAGlyTCC-1* deletion. For *tRNAGlyTCC-1-1* and *tRNAGlyTCC-1-7* single KO mice, we used WT littermates as control animals. For *tRNAGlyTCC-1-7*/*tRNAGlyTCC-1-5* double KOs, we used littermates heterozygous or WT at one or both *tRNAGlyTCC-1* genes as control animals.

Tunicamycin Injections

Two cohorts of adult WT C57BL/6J mice were injected intraperitoneally with 3 mg/kg tunicamycin (SML1287; Sigma-Aldrich) or vehicle. Mice were left undisturbed for 18 hours until sacrifice (ATF4 Western blot) or behavioral testing (forced swim test [FST]).

Western Blotting

Western blotting was performed as previously described (19) using the following antibodies: GLDC (1:250 or 1:100; Sigma-Aldrich), GCSH (1:2000; Proteintech), AMT (T-protein; 1:2000; Proteintech), DLD (L-protein; 1:1000; Novus Biologicals), ACTB (1:5000; Cell Signaling Technology), H3 (1:10,000; Novus Biologicals), ATF4 (1:1000; Cell Signaling Technology), EIF2A (1:1000; Cell Signaling Technology), and phospho-EIF2A (Ser 51; 1:1000; Cell Signaling Technology). Secondary antibodies were either a peroxidase-labeled secondary antibody (Rabbit: 1:10,000; Amersham ECL horseradish peroxidase–conjugated antibodies, Cytiva) or a fluorescent secondary antibody (Alexa Fluor 647-conjugated anti-rabbit IgG #711-605-152; Jackson Immuno Research Laboratories Inc.). For ATF4 Western blots, we used subcellular fractionation as described previously (19) to obtain nuclei for input. For all other Western blots, we used whole-cell lysate.

Y-Shaped Adapter Mature tRNA/Unique Molecular Identifier Sequencing

Y-shaped adapter mature tRNA sequencing was performed as previously described in Blaze *et al.* (19,20) and adapted from Shigematsu *et al.* (22). Y-shaped adapter mature tRNA sequencing data analysis was performed as previously described (19,20). Significant differences between experimental groups or genotypes were denoted at a raw $p < .05$.

Real-Time Quantitative Reverse Transcription Polymerase Chain Reaction

For real-time quantitative polymerase chain reaction (qPCR) to identify *Gldc* mRNA expression levels, total RNA was extracted

from mouse forebrain using Trizol reagent and reverse transcribed with the Superscript III Reverse Transcriptase before being subjected to TaqMan qPCR using TaqMan Universal Master Mix (Applied Biosystems) and TaqMan probes for *Gldc* with *Gapdh* as a housekeeping gene (Applied Biosystems). qPCR reactions were run in triplicates, and data were analyzed using the comparative cycle threshold method and normalized to the housekeeping gene and WT control animals. An unpaired *t* test was used to compare genotypes, and significance was denoted at $p < .05$.

Fluorometric Glycine Assay

Cortical tissue was used for the fluorometric glycine assay (Abcam; Sigma-Aldrich) following manufacturer's instructions. Briefly, 10 to 20 mg of fresh-frozen tissue was weighed and homogenized with a vibrating pestle in glycine assay buffer and then centrifuged to remove insoluble material. Lysate was added to 50 μL of master reaction mix, including glycine enzyme mix, developer, and probe, and reactions were performed in duplicates. A standard curve was generated using glycine standard from 0 to 0.5 nmol/well. Glycine concentration in each sample was determined using the standard curve. An unpaired *t* test was used to compare conditions or genotypes, and significance was denoted at $p < .05$.

Mass Spectrometry (Liquid Chromatography-Tandem Mass Spectometry)

Fresh-frozen mouse cortical tissue was homogenized with a vibrating pestle in buffer containing sodium dodecyl sulfate, HEPES, sucrose, and protease inhibitors and quantified using a BCA assay (Thermo Fisher). Liquid chromatography-tandem mass spectometry was performed at the Rockefeller Proteomics Resource Center as previously described (19).

Metabolomic Profiling of Amino Acids

Unbiased metabolomic profiling of amino acids was performed as described previously (19). Briefly, fresh-frozen mouse brain tissue was homogenized with a vibrating pestle on ice in 80% methanol with heavy amino acid mix standards (Cambridge Isotope Laboratories MSK-A2-1.2 mix). After centrifugation, supernatant was placed into a new tube and dried using a SpeedVac. Amino acid metabolomics and data analysis were performed at the Rockefeller Proteomics Resource Center as previously described (19).

Behavior

Behavioral testing was performed as previously described by Blaze *et al.* (19) including the open field test, elevated plus maze, tail suspension test (TST), FST, and contextual fear conditioning.

Glycine Förster Resonance Energy Transfer Sensor

The glycine Förster resonance energy transfer (FRET) sensor GlyFS was used in acute hippocampal slices from *Nsun2* KO and WT mice as described previously (23). GlyFS was anchored in extracellular space to biotinylated cell membranes using a biotin-streptavidin linker and pressure injected in stratum radiatum of hippocampal CA1 region via micropipette, which was also used for recording of local field potentials. The stimulation electrode was positioned 100 to 200 μm away from the region of interest that was selected in the area labeled by GlyFS excluding the recording pipette. To assess the resting levels of glycine, we calculated fluorescence intensity ratios (R_0 and R_{MAX}) before and after saturating the sensor by bath application of 5-mM glycine. R_0/R_{MAX} was used as an estimate of extracellular glycine resting levels. To assess glycine levels after neuronal activity, we used high-frequency stimulation (HFS) of Schaffer collateral–CA1 synapses simultaneously with GlyFS imaging.

Statistical Analyses

Statistical analyses were performed using GraphPad Prism 8.4.3 software. For Western blot, reverse transcriptase-qPCR, and fluorometric glycine assay results, unpaired *t* tests were used to compare genotypes or treatment groups. For behavioral tests, 2-way analyses of variance (ANOVAs) (genotype × sex) and 2-tailed *t* tests with Bonferroni correction as post hoc tests were used when appropriate. For fear conditioning, we used 2-way repeated-measures ANOVAs (genotype × conditioned stimulus presentation or context) and 2-tailed *t* tests with Bonferroni correction as post hoc tests when appropriate. Simple linear regression was performed to generate a standard curve on fluorometric glycine assay. Statistical significance was denoted by $p < .05$. All bar graphs are presented as the mean, with error bars representing the standard error of the mean, and include all individual data points.

RESULTS

GLDC Is Decreased in the *Nsun2* KO Brain

Neuronal ablation of *Nsun2* in the mouse forebrain is associated with a 2-fold increase in intracellular glycine (19). Increases in glycine levels in *Nsun2* KO mice were accompanied by increased levels of various proteins involved in glycine-serine biosynthesis (Figure 1A), but no changes to serine were detected, which is the direct precursor to glycine (19). We confirmed this glycine specificity further by calculating a glycine-to-serine ratio from previous metabolomics data (19), showing a significant increase in the *Nsun2* KO cortex compared with WT control mice ($t_6 = 13.57$, $p < .0001$) (Figure 1A). This suggests that there may be a deficit in the breakdown of glycine, producing an overabundance in *Nsun2* KO brains, which we have replicated here in a new set of mice ($n = 9$ WT/7 KO; *t* test: $t_{14} = 2.140$, $p = .025$, 1-tailed due to replication of 2 previous independent experiments) (19) (Figure 1A). Glycine degradation is performed by the glycine cleavage system (GCS), which is localized to the mitochondria and includes 4 proteins (GLDC or P-protein, GCSH or H-protein, DLD or L-protein, and AMT or T-protein) that facilitate the breakdown of glycine into smaller chemical products (24) (Figure 1A). While all 4 proteins operate in a complex, GLDC is the rate-limiting enzyme in the system. GLDC has been associated with various mutations producing neurodevelopmental phenotypes due to excess glycine (25,26). *Gldc* is most highly expressed in astrocytes but is also expressed at lower levels in multiple subtypes of neurons. This includes the cluster of glutamatergic neurons also expressing *Camk2a*, which is the cell type targeted by *Cre recombinase* in our

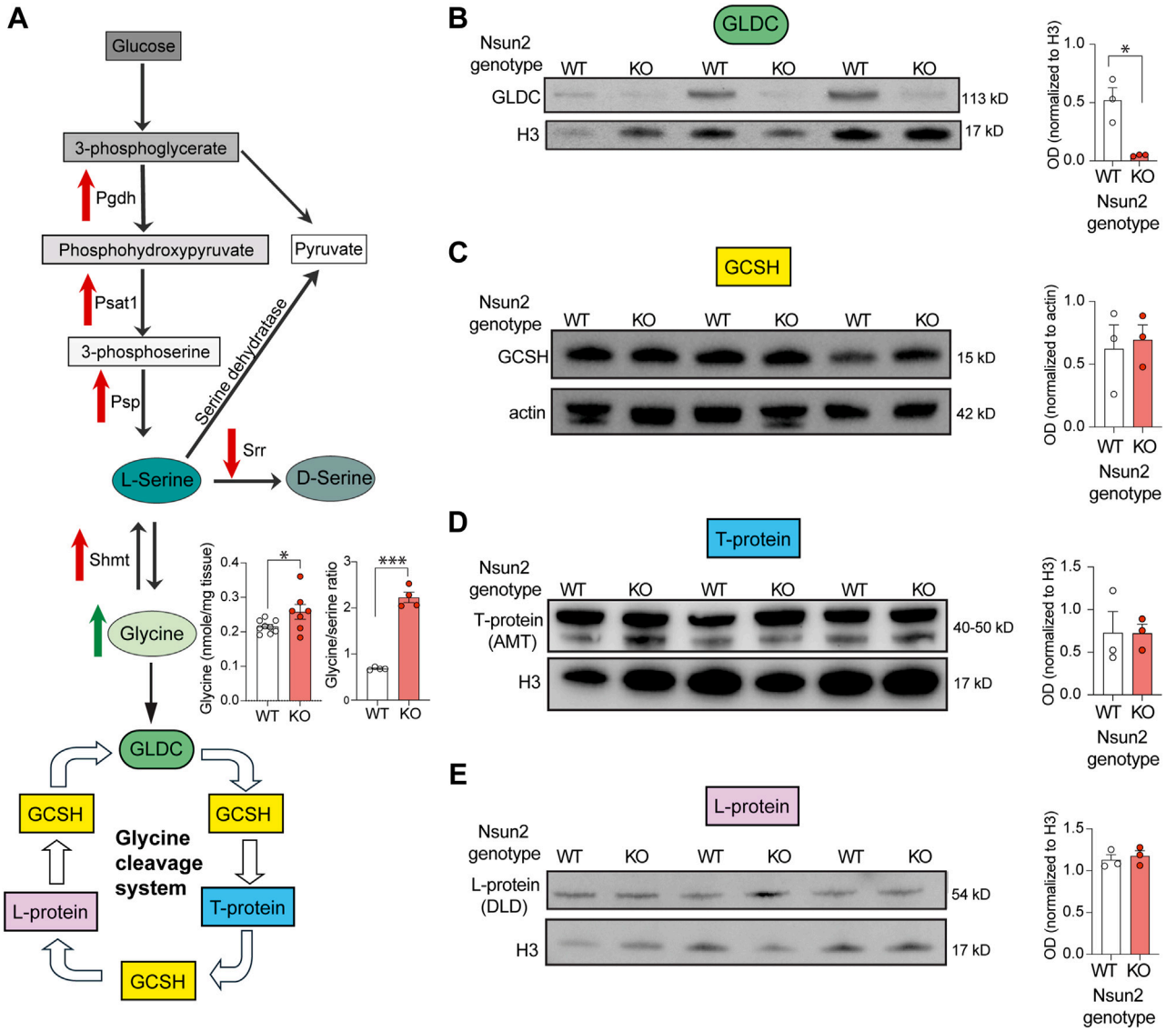

Figure 1. Dysregulation of the GCS in *Nsun2* KO mice. **(A)** Schematic of glycine-serine biosynthesis pathways that are significantly altered in *Nsun2* KO cortex as previously reported (19). Red arrows represent significant false discovery rate–adjusted p values $< .1$ in unbiased proteomic screen between *Nsun2* KO and WT cortex. Green arrow represents significantly changed amino acid concentration in KO vs. WT cortex. Using these data from (19), we also calculated glycine:serine ratios in the *Nsun2* KO cortex and found an increase for the KO vs. WT (n = 4/group; t_6 = 13.57, $p < .0001$). In a new cohort of mice, we also replicated the increase in glycine amino acid in *Nsun2* KO cortex using a fluorometric glycine assay (n = 8–9/group, t test, $^*p < .05$). Glycine is broken down by the GCS, which is depicted at the bottom of the schematic and consists of 4 proteins, including GLDC. **(B)** Western blot for GLDC in *Nsun2* KO and WT mouse cortex (n = 3/group, $^*p < .05$). **(C–E)** Western blots for 3 other GCS proteins, including **(C)** GCSH, **(D)** T-protein, and **(E)** L-protein, showing no difference in expression between *Nsun2* KO and WT brain (n = 3/group, t test, ps $>.05$). GCS, glycine cleavage system; GLDC, glycine decarboxylase; KO, knockout; OD, optical density; WT, wild-type.

Nsun2 KO mouse line (27–30) (Figure S1A–D). However, the role of GLDC in mature brain remains unresolved. Therefore, we examined whether these changes to glycine levels may be a mediator of the antidepressant-like phenotypes in the *Nsun2* mutant mice, as measured in behavioral despair paradigms.

First, we measured GLDC protein levels in the *Nsun2* KO brain using Western blotting. GLDC protein was almost undetectable in *Nsun2* KO frontal cortex compared with WT control mice (n = 3 WT/3 KO; t test: t_4 = 4.396, p = .012, 2-tailed) (Figure 1B), suggesting that loss of neuronal GLDC could be a potent driver of the glycine abundance in *Nsun2* KO brains. Then we measured the other 3 proteins involved in the GCS to identify whether these proteins were also decreased in the *Nsun2* KO brain (n = 3 WT/3 KO) (Figure 1B–E). In contrast to the large decrease in GLDC, we did not identify any significant changes in abundance of GCSH (t test: t_4 = 0.3204, p = .765, 2-tailed) (Figure 1C), T-protein (t test: t_4 = 0.021, p = .984, 2-tailed) (Figure 1D), or L-protein (t test: t_4 = 0.524, p = .628,

2-tailed) (Figure 1E) in the *Nsun2* KO brain, demonstrating the specificity of *Nsun2* deletion in depleting an individual component of the GCS to affect glycine levels.

Neuronal Depletion of *Gldc* Increases Glycine Abundance in Mouse Forebrain and Decreases Behavioral Despair

To identify whether loss of *Gldc* in forebrain neurons produces glycine overabundance and affects behavioral phenotypes in a manner that is similar to the *Nsun2* KO model, we developed a forebrain neuron-specific postnatal *Gldc* KO mouse. In these mice, exon 3 of *Gldc* is flanked by loxP sites (Figure 2A), and they were crossed with *Camk2a-Cre*+ mice for postnatal forebrain neuronal deletion of *Gldc*. Whole-cell lysate from adult *Gldc* KO mice showed a significant decrease in *Gldc* mRNA (n = 9 WT/5 KO; t test: t_{12} = 5.817, $p < .001$; 2-tailed) (Figure 2B) and protein, which was confirmed with both Western blot (n = 3 WT/3 KO; t test: t_4 = 3.726, p = .020, 2-tailed) (Figure 2C) and liquid chromatography-tandem mass spectometry (n = 8 WT/6 KO; glycine: fold change = 1.32, p = .017) (Figure 2D). We also measured protein expression of

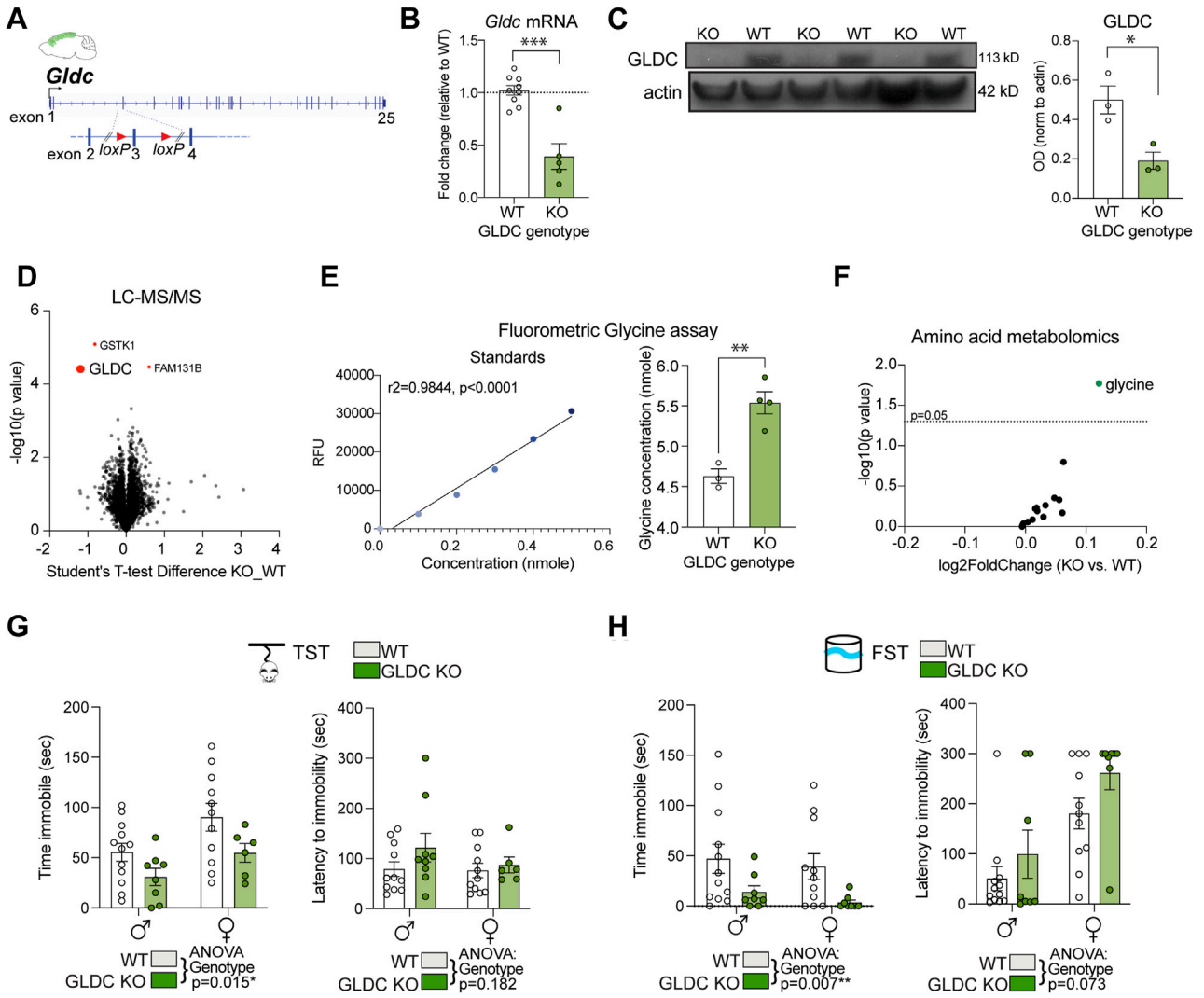

Figure 2. Molecular and behavioral effects of neuronal *Gldc* deletion in adult mice. **(A)** Gene structure of mouse *Gldc* with loxP sites surrounding exon 3. When crossed with *Camk2a-Cre* driver line, exon 3 is excised, leading to postnatal deletion of *Gldc* in most forebrain neurons. **(B)** Quantitative in mouse cortex using TaqMan probe for *Gldc* in KO vs. WT mice (n = 3/group, ***$p < .001$). **(C)** Western blot for GLDC in KO and WT mouse cortex (n = 3/group, *$p < .05$). **(D)** An unbiased proteomic screen of *Gldc* KO vs. WT cortex showed minimal changes but confirmed a significant downregulation of GLDC protein in KO mice (n = 4–5/group). **(E)** Fluorometric glycine assay showing increased glycine amino acid levels in *Gldc* KO mice (n = 4–5/group, **$p < .01$). **(F)** An unbiased screen of 16/20 amino acids showed a significant increase in glycine in *Gldc* KO cortex (n = 6–8/group). **(G, H)** Adult male and female *Gldc* KO and WT mice were tested for motivated escape behavior in the **(G)** TST and **(H)** FST (53). *Gldc* KO mice showed a significant decrease in amount of time immobile in the TST (n = 8–11/group, 2-way ANOVA, $p < .05$) and FST (n = 8–11/group, 2-way ANOVA, $p < .01$). ANOVA, analysis of variance; FST, forced swim test; GLDC, glycine decarboxylase; KO, knockout; LC-MS/MS, liquid chromatography-tandem mass spectometry; mRNA, messenger RNA; OD, optical density; RFU, relative fluorescence unit; TST, tail suspension test; WT, wild-type.

GCSH, another GCS protein, and found no significant difference between *Gldc* KO and WT mice, confirming the specificity of GLDC loss within the GCS (n = 3 WT/3 KO; t test: $t_4 = 1.656$, $p = .173$, 2-tailed) (Figure S2A). Then we confirmed this using both a targeted approach (n = 3 WT/4 KO; t test: $t_5 = 5.121$, $p = .004$, 2-tailed) (Figure 2E) and an unbiased metabolomic method (Figure 2F) in which glycine was selectively increased in *Gldc* KO brains compared with WT brains.

After confirming that neuronal *Gldc* deletion produced an excess of glycine in mouse forebrain, we wondered whether this was linked to altered behavioral phenotypes. *Gldc* KO mice had no gross neuroanatomical abnormalities or alterations in body weight compared with WT mice (n =13 male [M] WT, 10 female [F] WT/10 M KO, 6 F KO; 2-way ANOVA, genotype: $F_{1,35} = 2.043$, $p = .162$; sex: $F_{1,35} = 13.54$, $p < .001$; genotype-by-sex interaction: $F_{1,35} = 0.113$, $p = .739$) (Figure S2B). We performed behavioral tests for memory, anxiety-like behavior, and behavioral despair in adult *Gldc* KO and WT mice. We found no effect of genotype on acquisition of contextual fear (n = 7 WT/8 KO, 2-way ANOVA, $p = .152$) or retrieval of contextual fear after 24 hours (n = 7 WT/8 KO, 2-way ANOVA, $p = .462$) (Figure S2C). We likewise found no effect of *Gldc* KO on anxiety-like behavior in the open field test (n = 12 M WT, 11 F WT/8 M KO, 8 F KO; 2-way ANOVA, ps $> .05$) (Figure S2D) or elevated plus maze (n = 12 M WT, 11 F WT/8 M KO, 8 F KO; 2-way ANOVA, ps $> .05$) (Figure S2E). However, as predicted, *Gldc* KO mice showed a decrease in behavioral despair in 2 independent tests.

In the TST (Figure 2G), *Gldc* KO mice spent less time immobile (n = 11 M WT, 11 F WT/8 M KO, 6 F KO; 2-way ANOVA, genotype: $F_{1,33} = 6.650$, $p = .015$; sex: $F_{1,33} = 6.430$, $p = .016$; genotype-by-sex interaction: $F_{1,33} = 0.226$, $p = .637$), with no change in latency to immobility (genotype: $F_{1,33} = 1.854$, $p = .182$; sex: $F_{1,33} = 0.893$, $p = .351$; genotype-by-sex interaction: $F_{1,33} = 0.644$, $p = .428$). The decrease in behavioral despair was further confirmed in the FST (Figure 2H), in which *Gldc* KO mice likewise showed a decrease in the time spent immobile (n = 12 M WT, 11 F WT/8 M KO, 8 F KO; 2-way ANOVA, genotype: $F_{1,35} = 8.093$, $p = .007$; sex: $F_{1,35} = 0.564$, $p = .458$; interaction: $F_{1,35} = 0.010$, $p = .920$) and a trend-level increase in latency to immobility (genotype: $F_{1,35} = 3.765$, $p = .060$; sex: $F_{1,35} = 19.03$, $p = .001$; interaction: $F_{1,35} = 0.236$, $p = .630$). These results demonstrate a potent effect of glycine abundance mediated by neuronal *Gldc* expression on behavioral despair, recapitulating the effects seen in *Nsun2* KO mice (19), while other behavioral changes, including anxiety-like behaviors and cognition, were spared following *Gldc* deletion in neurons, in contrast to the *Nsun2* KO mice.

Loss of *Nsun2* Produces a Robust ISR in the Brain

Dysregulation of tRNA levels and amino acid content cause activation of the ISR in various cell lines and tissues (18), including brain (15,31), and has been linked to behavioral changes (15) (Figure 3A). Briefly, the ISR is activated when a stress signal, including amino acid and tRNA changes, activate enzymes that phosphorylate EIF2A, leading to global inhibition of protein synthesis while certain transcription factors with upstream open reading frames (i.e., ATF4) are activated to promote cell survival (18,32). Therefore, we investigated whether loss of *Nsun2* produces activation of the ISR in mouse cortex. First, we quantified ATF4 protein levels in nuclei from *Nsun2* KO forebrain. ATF4 is a transcription factor that is expressed only via an alternative transcription start site when the ISR is activated and EIF2A is phosphorylated, making it a very distinct hallmark of the ISR (18). We found that ATF4 was expressed robustly only in *Nsun2* KO nuclei and negligibly expressed in WT brains (n = 5 WT/5 KO, Mann-Whitney $U = 0$, $p = .008$, 2-tailed) (Figure 3B). To further confirm that the ISR was present, we measured phosphorylated EIF2A levels in whole-cell lysate and detected a significant increase in P-EIF2A in *Nsun2* KO forebrain compared with WT forebrain (n = 5 WT, 5 KO, t test: $t_8 = 3.401$, $p = .009$, 2-tailed) (Figure 3C). Taken together, these 2 molecular signatures confirm a robust ISR following ablation of *Nsun2* in forebrain neurons, which may be related to the neuropsychiatric-related phenotypes observed previously (19) in *Nsun2* KO mice.

We then wanted to further test whether an ISR activation could drive behavioral despair in the mouse model. To this end, we experimentally induced the ISR in WT adult male mice by systemic injection of tunicamycin, a well-established agent known to penetrate the blood-brain barrier, to induce phosphorylation of EIF2A and increase ATF4 in brain (33) (Figure 3D). We measured behavioral despair using the FST (Figure 3D) in mice injected intraperitoneally with single-dose 3 mg/kg tunicamycin and left undisturbed for 18 hours (a time point previously shown to be associated with a robust ISR in brain) (33). We confirmed for this time point that ATF4 was expressed at higher levels in tunicamycin-injected mice than in vehicle-injected control mice (n = 3 tunicamycin/2 vehicle) (Figure 3E). However, in contrast to the decrease in immobility observed in *Nsun2* KO mice (19), we observed that tunicamycin-injected mice showed a significantly increased time immobile (n = 10/condition; t test: $t_{18} = 2.561$, $p = .0197$, 2-tailed) and a marginally shorter latency to the first bout of immobility (n = 10/condition; t test: $t_{18} = 1.541$, $p = .1408$, 2-tailed) (Figure 3F). Additionally, we used amino acid metabolomics to assess whether ISR induction alters glycine levels in brain and found that there was no significant change to glycine levels, but 5 other amino acids (histidine, alanine, tyrosine, isoleucine, and tryptophan) were significantly altered following tunicamycin injection versus vehicle controls (Figure 3G). These results suggest that while *Nsun2* KO mice show a robust ISR, the ISR itself is not causally linked to the changes in glycine metabolism and alterations in the behavioral despair paradigm in *Nsun2* KO mice. However, we cannot rule out a possible role of chronic activation of the ISR caused by loss of *Nsun2* because our acute tunicamycin experiment mimics a short-term pharmacological treatment.

Depletion of *tRNAGlyTCC-1* Decreases Forebrain Glycine Levels but Does Not Decrease Behavioral Despair

Next, we asked whether a decrease in $tRNA^{Gly}$ supply may be an additional driver of the molecular and behavioral changes observed in *Nsun2*-deficient mice. However, $tRNA^{Gly}$ genes have a large amount of redundancy in the genome, with a total of 26 genes coding for the 4 isoacceptor families, and are

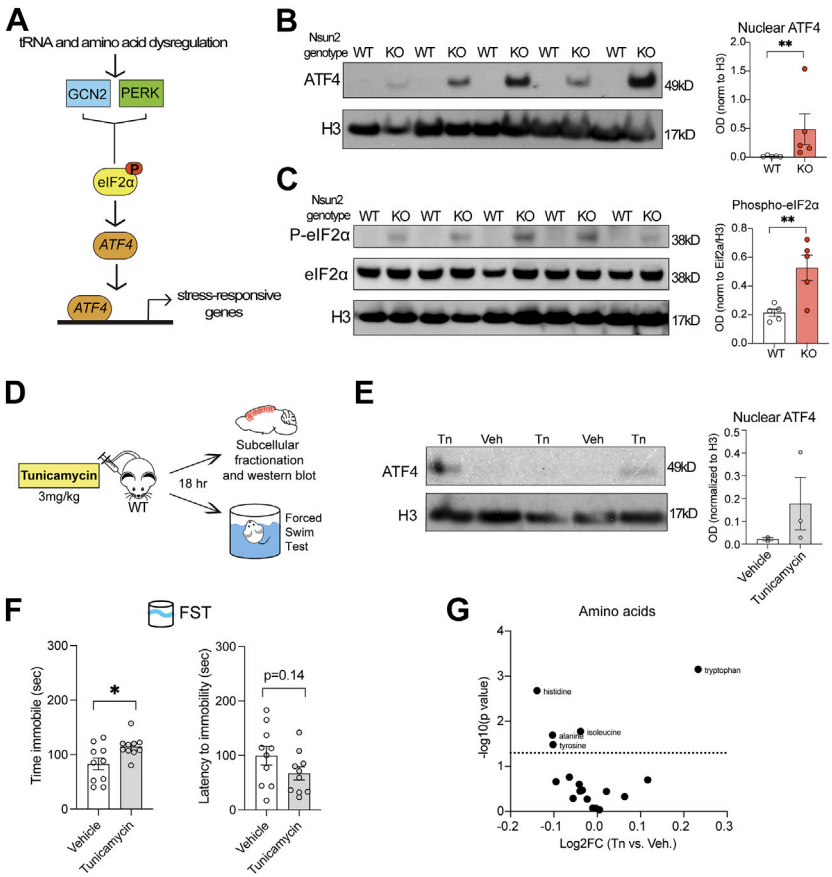

Figure 3. ISR as a potential mechanism for behavioral abnormalities in *Nsun2* KO mice. **(A)** Schematic of the ISR. The enzymes GCN2 or PERK are activated in response to dysregulation of tRNA or amino acid levels, leading to phosphorylation of EIF2A, which impairs global translation but induces translational processes for genes with upstream open reading frames, such as ATF4, which induces transcription of stress-responsive genes. **(B)** ATF4 protein in cortical nuclei isolated from adult *Nsun2* KO and WT mice and **(C)** phosphorylated EIF2A expression in whole-cell lysate. Note the robust activation of ISR in *Nsun2* KO (n = 5/group; t test; $^{**}p < .01$). **(D)** Schematic of experimental design for systemic tunicamycin administration for ISR induction in WT adult male mice. **(E)** ATF4 protein in cortical nuclei isolated from mice injected with tunicamycin or vehicle. **(F)** Behavioral despair was measured with the FST (53) 18 hours after tunicamycin injection. Tunicamycin-injected mice showed increased immobility in the FST (n = 10/group; t test; $^{*}p < .05$). **(G)** Unbiased metabolomics screen of amino acids in tunicamycin-treated vs. vehicle brains. FC, fold change; FST, forced swim test; ISR, integrated stress response; KO, knockout; OD, optical density; Tn, tunicamycin; tRNA, transfer RNA; Veh, vehicle; WT, wild-type.

localized to 9 different chromosomes (with 10/26 genes on chromosome 1), making the functionality and viability of one $tRNA^{Gly}$ gene deletion difficult. For example, for the $tRNA^{Gly}_{GCC}$ isoaccepter family, there are 4 different isodecoders with up to 8 genes in different genomic locations for each isodecoder (34). Therefore, we chose to focus on $tRNA^{Gly}_{TCC}$ because this isoacceptor was decreased in *Nsun2* KO, was also associated with altered codon-specific translation (19), and provided the most feasibility for deletion by having only one isodecoder expressed in mouse (*tRNAGlyTCC-1*) (34). Mice were generated using CRISPR/Cas9 with single-guide RNA targeted to the *tRNAGlyTCC-1* sequence (ACCCGGGTCAACTGCTTGGA). There are 7 copies of *tRNAGlyTCC-1* in the genome, and we generated 2 mouse lines with a single deletion in *tRNAGlyTCC-1-1* (Figure S3A, B) and *tRNAGlyTCC-1-7* (Figure S3C, D), respectively. tRNA sequencing on mouse cortex from both lines revealed no change in *tRNAGlyTCC-1* expression, suggesting that a single deletion within this tRNA gene is not sufficient to deplete mature tRNA expression.

Because a single deletion at *tRNAGlyTCC-1* did not deplete expression, we then generated a line that contained deletions at 2 different *tRNAGlyTCC-1* genes, including an 11–base pair deletion at *tRNAGlyTCC-1-5* and a 25–base pair deletion at *tRNAGlyTCC-1-7*, reasoning that perhaps deletions at 2 tRNA genes for *tRNAGlyTCC-1* would produce a considerable depletion in *tRNAGlyTCC-1* expression (Figure 4A). tRNA sequencing revealed a decrease in *tRNAGlyTCC-1* for 3 of 3 samples ($\log_2$ fold change = −0.21, unadjusted p = .053) with the double KO compared with WT and heterozygous control mice (n = 3 WT, 3 KO) (Figure 4B). While none of the tRNA isodecoder comparisons reached significance after false discovery rate correction, there were also 7 $tRNA^{Val}$ isodecoders marginally decreased in the *tRNAGlyTCC-1* double KO mice. We speculate that there may be a chromosomal loop or interaction between the genes coding for *tRNAGlyTCC-1* and the various $tRNA^{Val}$ isodecoder genes because while they are not located near our targeted deletions, other studies have shown long-range contacts of tRNA genes in non-neuronal cell types (35).

Alterations in the tRNA gene dosage have been shown to influence amino acid levels in brain of our *Nsun2* mutant line (19) and others (15,17). For example, deletion of *tRNA-Arg-TCT-4-1* in mice produced an increase in both serine and glycine amino acids in the hippocampus (15). Global hypomethylation across the tRNAome via *Nsun2* deletion also produced an increase in various amino acids including glycine and serine in mouse skin cells (17), and we previously showed approximately 150% increase in only glycine amino acid in brains of mice with depletion of m^5C and specifically $tRNA^{Gly}$ expression (19). For that reason, we wondered whether depletion of *tRNAGlyTCC-1* was associated with alterations in glycine amino acid. We used a fluorometric glycine assay to

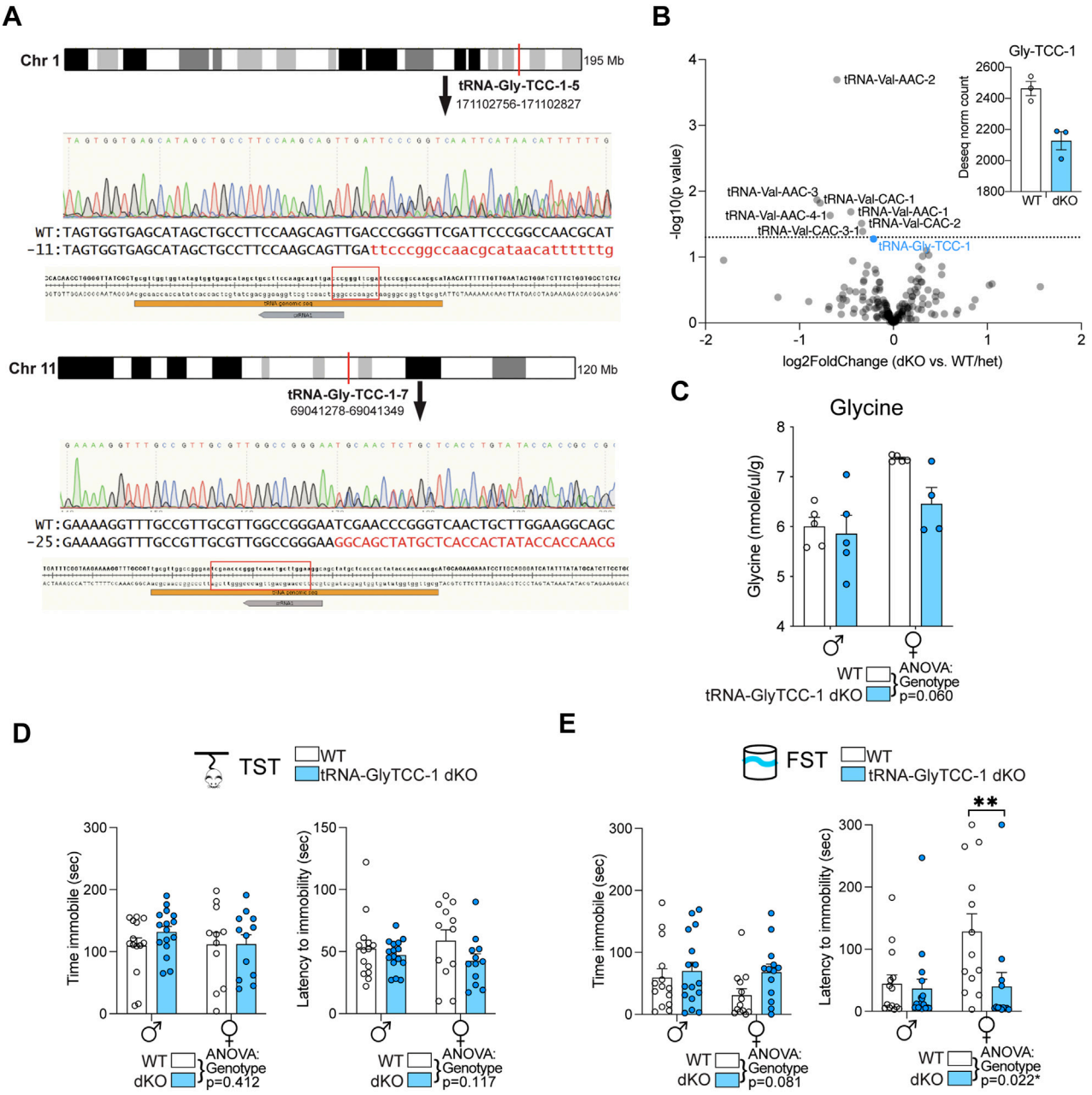

Figure 4. Molecular and behavioral effects of *tRNA-GlyTCC-1* deletion. **(A)** Chromosomal location of 2 *tRNA-Gly-TCC-1* genes harboring CRISPR/Cas9 deletions. The guide RNA is shown in gray below electropherograms targeting the *tRNA-Gly-TCC-1* family, and we detected a 1-bp deletion at *tRNA-Gly-TCC-1-5* (chr. 1) and a 10-bp deletion at *tRNA-Gly-TCC-1-7* (chr. 11). **(B)** YAMATseq was used as an unbiased screen of tRNA expression across the whole tRNAome and showed a decrease in *tRNA-Gly-TCC-1* expression in forebrain in *tRNA-GlyTCC-1* dKO mice but also significant decreases in multiple $tRNA^{Val}$ isodecoders (n = 3/group). **(C)** Glycine amino acid in mouse forebrain was measured with a fluorometric glycine assay in WT vs. dKO mice (n = 4–6/sex/genotype, 2-way ANOVA). One WT female outlier was excluded (Grubb's [alpha = 0.05], G = 2.036) **(D, E)** Adult male and female *tRNA-GlyTCC-1* KO and WT mice were tested for motivated escape behavior in the **(D)** TST and **(E)** FST (53). *tRNA-GlyTCC-1* dKO mice showed a significant decrease in latency to immobility in the FST (n = 11–16/group, 2-way ANOVA, $p < .05$), with *tRNA-GlyTCC-1* dKO females showing the most pronounced decrease (t test, $^{**}p < .01$). ANOVA, analysis of variance; dKO, double knockout; FST, forced swim test; tRNA, transfer RNA; TST, tail suspension test; WT, wild-type; YAMATseq, Y-shaped adapter mature tRNA sequencing.

measure glycine concentrations in forebrain of control and *tRNAGlyTCC-1* double KO mice and surprisingly found a trend-level decrease in glycine levels in the double KO mice compared with WT control mice (n = 5 M WT, 5 F WT/5 M KO, 4 F KO; 2-way ANOVA, genotype: $F_{1,15} = 4.129$, $p = .060$; sex: $F_{1,15} = 14.34$, $p = .002$; interaction: $F_{1,15} = 2.140$, $p = .164$; 1

WT female outlier excluded), particularly in female mice (Figure 4C), and no change in GLDC expression (n = 3 WT, 5 KO; t test: t_6 = 0.4426, p = .674, 2-tailed) (Figure S4A). These findings are in contrast to the *Nsun2* KO mice, which showed decreased $tRNA^{Gly}$ levels but increased glycine (19), suggesting that a decrease in $tRNA^{Gly}$ alone can alter glycine amino acid levels; however, the directionality of the change is model dependent, and the previously detected increase in glycine (19) is not a direct effect of the depletion of $tRNA^{Gly}$.

Next, we sought to determine whether decreases in *tRNAGlyTCC-1* and the accompanying decrease in glycine amino acid were associated with behavioral phenotypes, including behavioral despair. There were no gross anatomical abnormalities and no differences in body weight between WT and KO mice (Figure S4B) (n = 12 M WT, 7 F WT/11 M KO, 9 F KO; 2-way ANOVA, genotype: $F_{1,35}$ = 0.9896, p = .327; sex: $F_{1,35}$ = 57.39, $p < .001$; interaction: $F_{1,35}$ = 0.006, p = .939). Behavioral phenotyping for anxiety-like behavior using the open field test (n = 12 M WT, 4 F WT/14 M KO, 9 F KO) (Figure S4C) and elevated plus maze (n =12 M WT, 6 F WT/13 M KO, 11 F KO) (Figure S4D) revealed no significant changes between *tRNAGlyTCC-1* double KO mice and control mice (2-way ANOVAs, all ps $> .05$). To measure behavioral despair, we used the TST (Figure 4D) and found no significant differences in KO versus WT mice in the time spent immobile (n = 14 M WT, 11 F WT/16 M KO, 12 F KO; 2-way ANOVA, genotype: $F_{1,49}$ = 0.686, p = .411; sex: $F_{1,49}$ = 0.414, p = .523; interaction: $F_{1,49}$ = 0.614, p = .437) or latency to immobility (genotype: $F_{1,49}$ = 2.544, p = .117; sex: $F_{1,49}$ = 0.001, p = .977; interaction: $F_{1,49}$ = 0.602, p = .441). However, in another test of behavioral despair (and motivated escape behavior), the FST (Figure 4E), we detected a prodepressant phenotype. *tRNAGlyTCC-1* dKO mice showed a trend-level increase in the time spent immobile compared with WT control mice (n = 14 M WT, 13 F WT/16 M KO, 13 F KO; 2-way ANOVA, genotype: $F_{1,52}$ = 3.170, p = .081; sex: $F_{1,52}$ = 1.235, p = .271; interaction: $F_{1,52}$ = 0.967, p = .330). They also displayed a significantly shorter latency to immobility (genotype: $F_{1,52}$ = 5.537, p = .022; sex: $F_{1,52}$ = 4.593, p = .037; interaction: $F_{1,52}$ = 3.899, p = .054), with post hoc tests showing a significant decrease in latency to immobility for females specifically (t_{52} = 2.959, p = .009). These data suggest that neither male nor female double KO mice show the same antidepressant-like phenotype as *Nsun2* KO mice. Rather, depletion of *tRNAGlyTCC-1* produces an increase in behavioral despair coupled with a decrease in glycine, which are both inconsistent with our previous *Nsun2* KO model, that showed a depletion of $tRNA^{Gly}$ associated with an increase in glycine and a decrease in behavioral despair. We reason that this opposing pattern suggests that $tRNA^{Gly}$ may not be mediating the behavioral phenotypes observed; instead, glycine amino acid may be a target of interest that is altering behavioral phenotypes in both models. Furthermore, we noted that the other glycine tRNA isoacceptor families (mainly $tRNA^{Gly}_{CCC}$ and $tRNA^{Gly}_{GCC}$) are unaffected in the *tRNA-Gly-TCC-1* KO mice while they are dramatically depleted in the *Nsun2* KO mice (19), which produces a much milder effect on $tRNA^{Gly}$ levels overall, so we cannot eliminate the possibility that the severity of $tRNA^{Gly}$ depletion impacts the behavioral phenotype.

Changes in *Nsun2* KO Glycine Levels Do Not Reflect Extracellular Glycine

Thus far, both lines of investigation (ISR and $tRNA^{Gly}$) have suggested that these mechanisms alone are not causally related to behavioral phenotypes observed in the *Nsun2* KO mice, but alterations in glycine levels are a plausible alternative. We previously detected an approximately 150% increase in glycine levels in the cortex of *Nsun2* KO mice using amino acid metabolomics from whole-cell lysates (19), but due to the actions of glycine both intracellularly during protein synthesis and extracellularly as crucial components of excitatory synaptic transmission in NMDA receptor binding as well as binding to the glycine receptor, we were unable to detect whether changes in glycine were taking place inside or outside of neurons. To answer this question, we used a FRET-based optical indicator for glycine (GlyFS) (23), which was anchored to the extracellular surface of biotinylated cell membranes in acute slices using a biotin-streptavidin linker. For experiments, GlyFS was pressure injected in the stratum radiatum of the hippocampal CA1 region with a micropipette, which was also used for recording of local field potentials. A stimulation electrode was positioned 100 to 200 μm away from the region labeled with GlyFS (Figure 5A, B). We then performed simultaneous local field potential recordings and extracellular glycine measurements in acute hippocampal slices of adult *Nsun2* KO and WT mice.

To assess the resting levels of glycine, we calculated the GlyFS fluorescence intensity ratios R_0 and R_{MAX} before and after saturating GlyFS with 5 mM of exogenous glycine and used the ratio R_0/R_{MAX} as an estimate of extracellular glycine resting levels (33) (Figure 5C). Resting extracellular glycine levels in CA1 were not significantly different in WT and *Nsun2* KO mice (n = 18 WT/24 KO; t test: t_{40} = 0.93, p = .36, 2-tailed) (Figure 5D). HFS of Schaffer collateral–CA1 synapses was then performed simultaneously with GlyFS imaging to test whether activity-dependent extracellular glycine increases (33) are affected in *Nsun2* KO mice. Significant increases in extracellular glycine levels were observed in CA1 from WT mice (n = 13 independent experiments; paired t test: $t_{12} = -2.34$, p = .038, 2-tailed) (Figure 5E, left) and *Nsun2* KO mice (n = 23 independent experiments; paired t test: $t_{22} = -2.66$, p = .014, 2-tailed) (Figure 5F, left). No change was observed when HFS was omitted in CA1 of both WT mice (n = 13 independent experiments; t test: t_{12} = 0.53, p = .61, 2-tailed) (Figure 5E, right) and *Nsun2* KO mice (n = 23 independent experiments; t test: t_{22} = 0.49, p = .63, 2-tailed) (Figure 5F, right). Taken together, these results demonstrate that there are no detectable changes in extracellular glycine at baseline or in response to HFS in the *Nsun2* KO hippocampus, suggesting that the changes of total brain glycine content observed previously (19) are likely intracellular. Additionally, although we measured hippocampal glycine levels in the current experiment due to well-established synaptic transmission for optimal use of the GlyFS, it is likely that these findings are similar in other forebrain regions harboring *Nsun2* deletion, including the cortex, which will be a future area of study. To further investigate whether extracellular mediators of glycine activity, such as genes coding for glycine receptors and glutamate NMDA receptors, were differentially expressed in the *Nsun2* KO cortex, we leveraged previous RNA sequencing data from our group

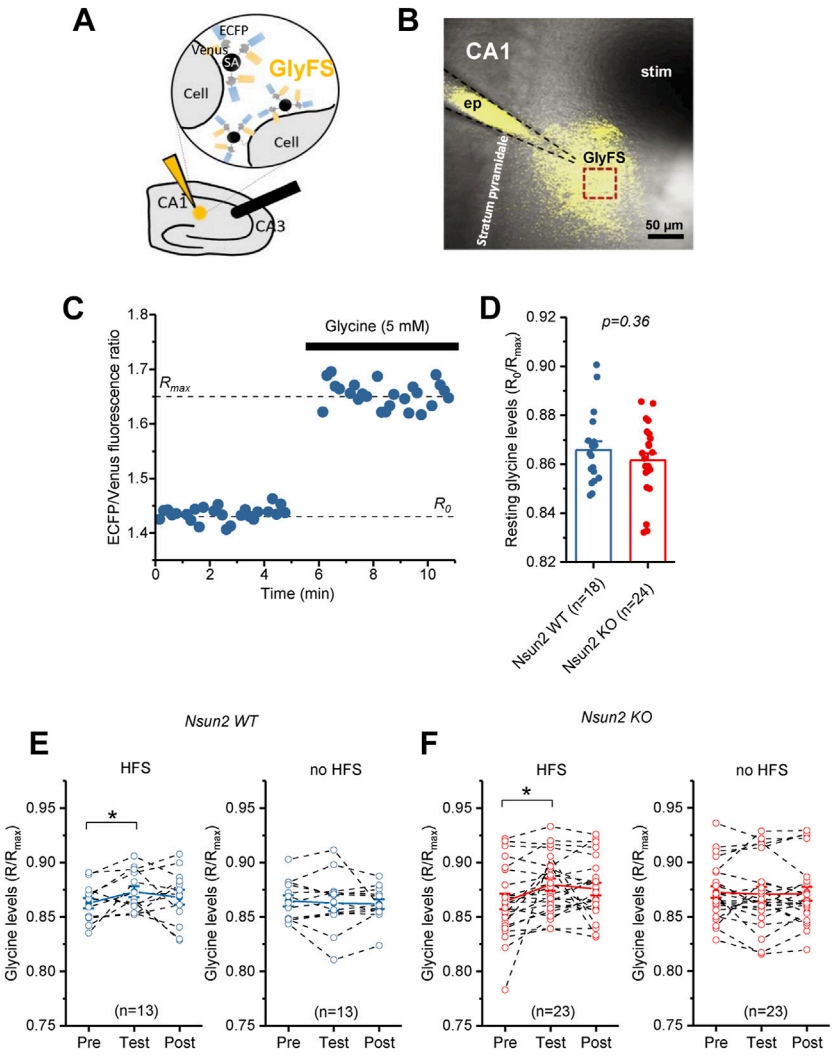

Figure 5. Neuronal *Nsun2* deletion does not alter extracellular glycine levels in the hippocampal CA1 region. **(A)** Schematic diagram of the experimental design. Glycine levels were measured using the Förster resonance energy transfer–based (FRET) sensor GlyFS in parallel to local field potentials in acute hippocampal slices. GlyFS was anchored in extracellular space to biotinylated cell membranes using a biotin-streptavidin linker. **(B)** GlyFS was pressure injected in stratum radiatum of hippocampal CA1 region via micropipette (ep). The same pipette was used for recording of local field potentials. Stimulation electrode (stim) was positioned 100 to 200 µm away from the region of interest (red dashed box) that was selected in the area labeled by GlyFS excluding the recording pipette. **(C)** To assess resting levels of glycine, we calculated fluorescence intensity ratios (R_0 and R_{MAX}) before and after saturating the sensor by bath application of 5-mM glycine. Then R_0/R_{MAX} was used as an estimate of extracellular glycine resting levels. **(D)** Resting extracellular glycine levels in CA1 were not significantly different in WT and *Nsun2* KO mice (n = 18 WT/24 KO; Student's t test, t_{40} = 0.93, p = .36, 2-tailed). **(E, F)** HFS of Schaffer collateral-CA1 synapses was performed simultaneously with GlyFS imaging. The pretest baseline, test response, and posttest levels (R/R_{MAX}) were determined. A significant increase in extracellular glycine levels was observed in CA1 from WT mice (n = 13 independent experiments; paired Student's t test: t_{12} = −2.34, p = .038, 2-tailed) **(E)** (left panel) and *Nsun2* KO mice (n = 23 independent experiments; paired Student t test: t_{23} = −2.66, p = .014, 2-tailed) **(F)** (left panel). No change was observed when HFS was omitted in CA1 of both WT mice (n = 13 independent experiments; paired Student's t test: t_{12} = 0.53, p = .61, 2-tailed) **(E)** (right panel) and *Nsun2* KO mice (n = 23 independent experiments; paired Student's t test: t_{22} = 0.49, p = .63, 2-tailed) **(F)** (right panel). Each data point represents an independent experiment. Error bars represent the SEM. *p < .05. HFS, high-frequency stimulation; KO, knockout; WT, wild-type.

(19). We found no changes to expression of glycine receptor genes (*Glra1*, *Glra2*, *Glra3*, *Glra4*, *Glrb*) and no changes in expression for most of the NMDA receptor subunit genes (*Grin1*, *Grin2a*, *Grin2b*, *Grin2c*, *Grin2d*, *Grin3a*) (Table S1). However, we did find a significant increase in expression of *Grin3b* (log fold change = 1.504, adjusted p = .049), which encodes a subunit of the NMDA receptor involved in glycine binding. Because only one of the 12 genes coding for components of extracellular glycine binding shows an alteration in the *Nsun2* KO cortex, it is likely that the cortex, like the hippocampus, shows mainly intracellular changes in glycine.

DISCUSSION

Neuronal Glycine Metabolism as a Novel Target for Neuropsychiatric Phenotypes

Here, we identify glycine metabolism in mature forebrain neurons as a potential therapeutic target to elicit changes in behavioral despair in a mouse model. Specifically, conditional ablation of *Gldc* in mature forebrain neurons increased motivational escape behaviors in the FST and TST. It is important to note that these tests inform about antidepressant-like phenotypes, and their predictive validity in this regard both in pharmacological (36,37) and genetic (38) contexts could point to neuronal glycine regulation as a novel therapeutic avenue for the treatment of depression. We do acknowledge that the use of behavioral despair tests has drawbacks, such as arguments about an animal's adaptive energy conservation mechanism that could explain immobility or the view of these tests as measuring an animal's coping during an acute stressor, but capturing aspects of depression is a particularly challenging area of animal research (39). Other tests for depressive-like behavior including anhedonia or social avoidance after chronic defeat also have drawbacks and measure various other aspects of the full human depression phenotype. Remarkably, however, a case of familial bipolar depression has been linked to a rare supernumerary marker chromosome carrying copies of *GLDC* and the surrounding genes (40), and

furthermore, multiple lines of mutant mice with varying excess copies and overexpression of the *Gldc* gene show cognitive alterations and anxiety- and depression-related behaviors (41). Among other behavioral alterations, this includes a significant decrease in motivational escape behaviors (41) and therefore a phenotype opposite of the one that we report here for mice with neuron-specific *Gldc* ablation. The fact that a general oversupply of *Gldc* is associated with a depression-relevant behavioral phenotype in humans and mice while neuronal *Gldc* deficiency is associated with opposite changes in the same set of behavioral despair tests strongly speaks to the GCS, a multienzyme complex with GLDC as its rate-limiting molecule (42), as a potential target for the treatment of depression and psychosis. To further solidify GLDC as a potential target for neuropsychiatric investigation, future studies will investigate other animal models of depression, including chronic stress, and test of behavioral measures including efficacy of an antidepressant compared with the behavioral changes we observed.

Currently, however, the precise mechanisms linking the disruption of the neuronal GCS to changes in behavioral despair remain unclear. According to the current study, the dynamic fluctuations of glycine in the hippocampal extracellular space are fully maintained at baseline and in the context of synaptic plasticity–inducing electrical stimulation. However, this finding does not rule out glycinergic modulation of synaptic or extrasynaptic NMDA receptors as a frequently discussed mechanism in the context of antidepressant-like actions of glycine reuptake inhibitors (43–45). The question also remains: How does loss of *Nsun2* deplete GLDC? We expect that loss of *Nsun2* may cause GLDC reduction due to high glycine content of GLDC or potential posttranslational regulation of GLDC. Glycine amino acid content for GLDC is approximately 9.1%, while the average glycine content across the proteome is approximately 6.6%, and our previous work showed that *Nsun2*-related depletion of $tRNA^{Gly}$ causes impaired translation of glycine-rich proteins. Future studies should mechanistically explore the translational dynamics of GLDC in relation to loss of $tRNA^{Gly}$ (19). Furthermore, Nsun2 has also been shown to catalyze methylation on a subset of mRNAs, but to our knowledge, other groups have not shown cytosine methylation on *Gldc* mRNA in rodent brain (46). We also emphasize that behavioral profiles of the *Nsun2* KO mouse defined previously (19) are not completely consistent with the *Gldc* KO mouse presented in this study. While we observed a similar behavioral despair-like phenotype, the *Nsun2* KO mouse also exhibits changes in anxiety-like behavior and cognition (19), which are behavioral realms unaffected in the *Gldc* KO mouse. These changes are likely related to the additional molecular phenotypes present in *Nsun2* KO mice (which are also absent in the *Gldc* KO mice), including a dramatically altered proteome, depletion of $tRNA^{Gly}$, and a robust ISR induction.

Neuronal Glycine Metabolism Is Linked to *Nsun2*-Dependent Regulation of $tRNA^{Gly}$

Our goal in this study was to more mechanistically link NSUN2 epitranscriptomic tRNA regulation to complex behavioral phenotypes related to neuropsychiatric outcomes observed in neuronal *Nsun2* KO mice (19). *Nsun2* KO mice had a dramatic ~150% increase in glycine levels, which we have now shown is associated with severe impairment of the GCS, namely loss of the rate-limiting enzyme GLDC. In a new mouse model, we have now shown that conditional ablation of *Gldc* in neurons likewise produced an increase in glycine levels and a similar change in behavioral despair as the *Nsun2* KO mouse, suggesting that glycine levels and GCS are major contributors to complex behavioral outcomes following disruption of the NSUN2-mediated epitranscriptome.

Additional molecular alterations were present in *Nsun2* KO mice, including a selective decrease in $tRNA^{Gly}$ that was likely due to hypomethylation of the 4 NSUN2-mediated cytosine methylation sites at this tRNA isoacceptor family (19). Therefore, we tried to model this finding in isolation of other molecular changes by generating a novel mouse line with CRISPR/Cas9 deletion of $tRNA^{Gly}_{TCC}$. While a single gene deletion was not sufficient to decrease expression of the mature $tRNA^{Gly}_{TCC}$ isodecoder, deletion of 2 (of 7 total) genes coding for $tRNA^{Gly}_{TCC}$ caused a subtle decrease in $tRNA^{Gly}_{TCC}$ expression levels. Previous studies have shown that deletion of a single tRNA gene ($tRNA^{Arg}_{TCT}$) can have potent effects on tRNA expression and neurological phenotypes (15), but the difference in effect sizes between these studies and our model may depend on the specific tRNA being targeted and the number of isodecoders and genes available for that tRNA. Nevertheless, we showed here that subtle defects in tRNA gene dosage produce changes in behavioral despair.

It is widely established that dysregulation of amino acids and tRNAs can produce the ancient, evolutionarily conserved ISR, in which phosphoactivation of EIF2A triggers transcription of ATF4 and other transcription factors with upstream open reading frames to guide translation toward ensuring cell survival (15,18,31,47). We identified activation of the ISR in the *Nsun2* KO brain. Through our mechanistic experiments inducing ISR systemically in WT mice, we concluded that ISR activation alone is not sufficient to alter glycine levels or decrease behavioral despair, suggesting that alternate mechanisms are at play in the *Nsun2* KO mouse. While there is a thorough body of work on the ISR in brain in the context of cognition and neurodegeneration (32,33,48–51), we have now also provided a potential new downstream phenotypic consequence of ISR induction that warrants further study. It will also be of interest in the future to investigate our genetic manipulations, such as loss of *Gldc* or $tRNA^{Gly}$, in the context of the ISR.

Conclusions

Historically, there has been evidence for the importance of tRNA regulation in brain metabolism through phenotypic exploration of monogenic neurodevelopmental and neurodegenerative diseases associated with rare mutations in tRNA modification genes (52). More recently, evidence has demonstrated previously unrecognized potential for the tRNA regulome to be implicated in complex behaviors related to neuropsychiatric disease (52). Using 3 different molecular interventions ($tRNA^{Gly}$ expression, ISR induction, GCS impairment), we showed here that dysregulation of the tRNA regulome can have profound effects on cognition and complex behavior (see Table 1 for a summary). However, only a single factor was linked to decreased behavioral despair:

Table 1. Summary of Mouse Models With Molecular and Behavioral Findings

Mouse Model vs. Control	$tRNA^{Gly}$	Glycine Amino Acid	Motivated Escape Behavior
Nsun2 KO	↓	↑	↑
Gldc KO	n/a	↑	↑
tRNA-Gly-TCC dKO	↑	↑	↓
Wild-type systemic tunicamycin injection	n/a	No change	↓

Arrow thickness denotes significance. Thin arrows denote $p < .1$, and thick arrows denote $p < .05$.

dKO, double knockout; Gly, glycine; n/a, not applicable; tRNA, transfer RNA.

upregulation of neuronal glycine elicited by disruption of the GCS's rate-limiting enzyme, GLDC.

Further studies are warranted to identify how intracellular glycine and GCS impairment impacts behavior because this may provide a new therapeutic avenue outside of the already established roles of extracellular glycine function via pharmacological agents such as sarcosine treatment, which inhibits GlyT1 (14,43,44). In conclusion, we have demonstrated through rigorous methodologies that while multiple molecular signatures are at play following dysregulation of the tRNA epitranscriptome, including the ISR and changes in $tRNA^{Gly}$ levels, neuronal glycine metabolism is the most likely mechanism governing changes to complex behaviors relating to neuropsychiatric disease.

ACKNOWLEDGMENTS AND DISCLOSURES

This work was supported by a American Foundation for Suicide Prevention Young Investigator Grant (Grant No. YIG-1-013-21 [to JB]), a Mount Sinai Alzheimer's Disease Research Center REC grant (to JB), the National Institutes of Health (Grant No. R01DA054526 [to SA]), and the Germany Research Foundation (Grants Nos. HE6949/5 and HE6949/8 [to CH]).

JB and SA conceptualized the study and wrote the manuscript. JB performed mouse behavior experiments and molecular assays and analyzed data. VDE maintained transgenic mouse lines, genotyped, and helped with behavioral experiments. JAFP, PU, and CH performed glycine sensor experiments and analyzed data. BJ aided in tunicamycin ISR mouse experiments. SH, HA, and HM performed and analyzed liquid chromatography-tandem mass spectometry and amino acid metabolomics experiments. ZP and DC provided expertise for fear conditioning experiments.

We thank Dr. Rebecca Boumil and the team at the Jackson Laboratory for their expertise and generation of the *tRNA-GlyTCC-1* KO mouse lines. We also thank Dr. Andrew Chess for providing sequencing equipment.

The authors report no biomedical financial interests or potential conflicts of interest.

ARTICLE INFORMATION

From the Department of Psychiatry, Friedman Brain Institute, Icahn School of Medicine at Mount Sinai, New York, New York (JB, VDE, BJ, SA); Department of Neuroscience, Friedman Brain Institute, Icahn School of Medicine at Mount Sinai, New York, New York (JB, ZP, DC, SA); Institute of Cellular Neurosciences, University of Bonn, Bonn, Germany (JAFP, PU, CH); Proteomics Resource Center, The Rockefeller University, New York, New York (SH, HA, HM); and German Center for Neurodegenerative Diseases, Bonn, Germany (CH).

Address correspondence to Jennifer Blaze, Ph.D., at jenniferblaze@gmail.com.

Received Oct 4, 2024; revised Nov 7, 2024; accepted Dec 1, 2024.

Supplementary material cited in this article is available online at https://doi.org/10.1016/j.bpsgos.2024.100432.

REFERENCES

1. Paul SM, Potter WZ (2024): Finding new and better treatments for psychiatric disorders. Neuropsychopharmacology 49:3–9.
2. Howes OD, Thase ME, Pillinger T (2022): Treatment resistance in psychiatry: State of the art and new directions. Mol Psychiatry 27:58–72.
3. Sethi S, Wakeham D, Ketter T, Hooshmand F, Bjornstad J, Richards B, *et al.* (2024): Ketogenic diet intervention on metabolic and psychiatric health in bipolar and schizophrenia: A pilot trial. Psychiatry Res 335:115866.
4. Tajan M, Hennequart M, Cheung EC, Zani F, Hock AK, Legrave N, *et al.* (2021): Serine synthesis pathway inhibition cooperates with dietary serine and glycine limitation for cancer therapy. Nat Commun 12:366.
5. Maddocks ODK, Berkers CR, Mason SM, Zheng L, Blyth K, Gottlieb E, Vousden KH (2013): Serine starvation induces stress and p53-dependent metabolic remodelling in cancer cells. Nature 493:542–546.
6. Kawai N, Bannai M, Seki S, Koizumi T, Shinkai K, Nagao K, *et al.* (2012): Pharmacokinetics and cerebral distribution of glycine administered to rats. Amino Acids 42:2129–2137.
7. Kaufman MJ, Prescot AP, Ongur D, Evins AE, Barros TL, Medeiros CL, *et al.* (2009): Oral glycine administration increases brain glycine/creatine ratios in men: A proton magnetic resonance spectroscopy study. Psychiatry Res 173:143–149.
8. Bannai M, Kawai N, Nagao K, Nakano S, Matsuzawa D, Shimizu E (2011): Oral administration of glycine increases extracellular serotonin but not dopamine in the prefrontal cortex of rats. Psychiatry Clin Neurosci 65:142–149.
9. Bannai M, Kawai N, Ono K, Nakahara K, Murakami N (2012): The effects of glycine on subjective daytime performance in partially sleep-restricted healthy volunteers. Front Neurol 3:61.
10. Heresco-Levy U, Javitt DC, Ermilov M, Mordel C, Silipo G, Lichtenstein M (1999): Efficacy of high-dose glycine in the treatment of enduring negative symptoms of schizophrenia. Arch Gen Psychiatry 56:29–36.
11. Leiderman E, Zylberman I, Zukin SR, Cooper TB, Javitt DC (1996): Preliminary investigation of high-dose oral glycine on serum levels and negative symptoms in schizophrenia: An open-label trial. Biol Psychiatry 39:213–215.
12. Strzelecki D, Kropiwnicki P, Rabe-Jabłońska J (2013): Augmentation of antipsychotics with glycine may ameliorate depressive and extrapyramidal symptoms in schizophrenic patients: A preliminary 10-week open-label study. Psychiatr Pol 47:609–620.
13. Kawai N, Sakai N, Okuro M, Karakawa S, Tsuneyoshi Y, Kawasaki N, *et al.* (2015): The sleep-promoting and hypothermic effects of glycine are mediated by NMDA receptors in the suprachiasmatic nucleus. Neuropsychopharmacology 40:1405–1416.
14. Peyrovian B, Rosenblat JD, Pan Z, Iacobucci M, Brietzke E, McIntyre RS (2019): The glycine site of NMDA receptors: A target for cognitive enhancement in psychiatric disorders. Prog Neuropsychopharmacol Biol Psychiatry 92:387–404.
15. Kapur M, Ganguly A, Nagy G, Adamson SI, Chuang JH, Frankel WN, Ackerman SL (2020): Expression of the neuronal tRNA n-Tr20 regulates synaptic transmission and seizure susceptibility. Neuron 108:193–208.e9.

16. Ishimura R, Nagy G, Dotu I, Zhou H, Yang XL, Schimmel P, *et al.* (2014): RNA function. Ribosome stalling induced by mutation of a CNS-specific tRNA causes neurodegeneration. Science 345:455–459.
17. Gkatza NA, Castro C, Harvey RF, Heiß M, Popis MC, Blanco S, *et al.* (2019): Cytosine-5 RNA methylation links protein synthesis to cell metabolism. PLoS Biol 17:e3000297.
18. Costa-Mattioli M, Walter P (2020): The integrated stress response: From mechanism to disease. Science 368:eaat5314.
19. Blaze J, Navickas A, Phillips HL, Heissel S, Plaza-Jennings A, Miglani S, *et al.* (2021): Neuronal Nsun2 deficiency produces tRNA epitranscriptomic alterations and proteomic shifts impacting synaptic signaling and behavior. Nat Commun 12:4913.
20. Blaze J, Browne CJ, Futamura R, Javidfar B, Zachariou V, Nestler EJ, Akbarian S (2024): tRNA epitranscriptomic alterations associated with opioid-induced reward-seeking and long-term opioid withdrawal in male mice. Neuropsychopharmacology 49:1276–1284.
21. Kim YA, Siddiqui T, Blaze J, Cosacak MI, Winters T, Kumar A, *et al.* (2023): RNA methyltransferase NSun2 deficiency promotes neurodegeneration through epitranscriptomic regulation of tau phosphorylation. Acta Neuropathol 145:29–48.
22. Shigematsu M, Honda S, Loher P, Telonis AG, Rigoutsos I, Kirino Y (2017): YAMAT-seq: An efficient method for high-throughput sequencing of mature transfer RNAs. Nucleic Acids Res 45:e70.
23. Zhang WH, Herde MK, Mitchell JA, Whitfield JH, Wulff AB, Vongsouthi V, *et al.* (2018): Monitoring hippocampal glycine with the computationally designed optical sensor GlyFS. Nat Chem Biol 14:861–869.
24. Kikuchi G (1973): The glycine cleavage system: Composition, reaction mechanism, and physiological significance. Mol Cell Biochem 1:169–187.
25. Kure S, Takayanagi M, Narisawa K, Tada K, Leisti J (1992): Identification of a common mutation in Finnish patients with nonketotic hyperglycinemia. J Clin Invest 90:160–164.
26. Kure S, Narisawa K, Tada K (1991): Structural and expression analyses of normal and mutant mRNA encoding glycine decarboxylase: Three-base deletion in mRNA causes nonketotic hyperglycinemia. Biochem Biophys Res Commun 174:1176–1182.
27. Allen Institute for Brain Science (2004): Allen Mouse Brain Atlas. Available at: mouse.brain-map.org. Accessed August 1, 2024.
28. Yao Z, van Velthoven CTJ, Kunst M, Zhang M, McMillen D, Lee C, *et al.* (2023): A high-resolution transcriptomic and spatial atlas of cell types in the whole mouse brain. Nature 624:317–332.
29. Lein ES, Hawrylycz MJ, Ao N, Ayres M, Bensinger A, Bernard A, *et al.* (2007): Genome-wide atlas of gene expression in the adult mouse brain. Nature 445:168–176.
30. Allen Institute for Brain Science (2023): Allen Brain Cell Atlas. RRID: SCR_024440. Available at: https://portal.brain-map.org/atlases-and-data/bkp/abc-atlas. Accessed August 1, 2024.
31. Zuko A, Mallik M, Thompson R, Spaulding EL, Wienand AR, Been M, *et al.* (2021): tRNA overexpression rescues peripheral neuropathy caused by mutations in tRNA synthetase. Science 373:1161–1166.
32. Pakos-Zebrucka K, Koryga I, Mnich K, Ljujic M, Samali A, Gorman AM (2016): The integrated stress response. EMBO Rep 17:1374–1395.
33. Helseth AR, Hernandez-Martinez R, Hall VL, Oliver ML, Turner BD, Caffall ZF, *et al.* (2021): Cholinergic neurons constitutively engage the ISR for dopamine modulation and skill learning in mice. Science 372: eabe1931.
34. Chan PP, Lowe TM (2016): GtRNAdb 2.0: An expanded database of transfer RNA genes identified in complete and draft genomes. Nucleic Acids Res 44:D184–D189.
35. Van Bortle K, Phanstiel DH, Snyder MP (2017): Topological organization and dynamic regulation of human tRNA genes during macrophage differentiation. Genome Biol 18:180.
36. Herzog DP, Beckmann H, Lieb K, Ryu S, Müller MB (2018): Understanding and predicting antidepressant response: Using animal models to move toward precision psychiatry. Front Psychiatry 9:512.
37. Wang Q, Timberlake MA, Prall K, Dwivedi Y (2017): The recent progress in animal models of depression. Prog Neuropsychopharmacol Biol Psychiatry 77:99–109.
38. El Yacoubi M, Altersitz C, Latapie V, Rizkallah E, Arthaud S, Bougarel L, *et al.* (2024): Two polygenic mouse models of major depressive disorders identify TMEM161B as a potential biomarker of disease in humans. Neuropsychopharmacology 49:1129–1139.
39. Gencturk S, Unal G (2024): Rodent tests of depression and anxiety: Construct validity and translational relevance. Cogn Affect Behav Neurosci 24:191–224.
40. Grochowski CM, Gu S, Yuan B, Tcw J, Brennand KJ, Sebat J, *et al.* (2018): Marker chromosome genomic structure and temporal origin implicate a chromoanasynthesis event in a family with pleiotropic psychiatric phenotypes. Hum Mutat 39:939–946.
41. Kambali M, Li Y, Unichenko P, Feria Pliego JA, Yadav R, Liu J, *et al.* (2024): An increased copy number of glycine decarboxylase (GLDC) associated with psychosis reduces extracellular glycine and impairs NMDA receptor function [published online Aug 30]. Mol Psychiatry.
42. Pai YJ, Leung KY, Savery D, Hutchin T, Prunty H, Heales S, *et al.* (2015): Glycine decarboxylase deficiency causes neural tube defects and features of non-ketotic hyperglycinemia in mice. Nat Commun 6:6388.
43. Huang C-C, Wei I-H, Huang C-L, Chen K-T, Tsai M-H, Tsai P, *et al.* (2013): Inhibition of glycine transporter-I as a novel mechanism for the treatment of depression. Biol Psychiatry 74:734–741.
44. Chen K-T, Wu C-H, Tsai M-H, Wu Y-C, Jou M-J, Huang C-C, Wei I-H (2017): Antidepressant-like effects of long-term sarcosine treatment in rats with or without chronic unpredictable stress. Behav Brain Res 316:1–10.
45. Mathew SJ (2013): Glycine transporter-I inhibitors: A new class of antidepressant? Biol Psychiatry 74:710–711.
46. Amort T, Rieder D, Wille A, Khokhlova-Cubberley D, Riml C, Trixl L, *et al.* (2017): Distinct 5-methylcytosine profiles in poly(A) RNA from mouse embryonic stem cells and brain. Genome Biol 18:1.
47. Spaulding EL, Hines TJ, Bais P, Tadenev ALD, Schneider R, Jewett D, *et al.* (2021): The integrated stress response contributes to tRNA synthetase-associated peripheral neuropathy. Science 373:1156–1161.
48. Mallucci GR, Klenerman D, Rubinsztein DC (2020): Developing therapies for neurodegenerative disorders: Insights from protein aggregation and cellular stress responses. Annu Rev Cell Dev Biol 36:165–189.
49. Chou A, Krukowski K, Jopson T, Zhu PJ, Costa-Mattioli M, Walter P, Rosi S (2017): Inhibition of the integrated stress response reverses cognitive deficits after traumatic brain injury. Proc Natl Acad Sci U S A 114:E6420–E6426.
50. Oliveira MM, Mohamed M, Elder MK, Banegas-Morales K, Mamcarz M, Lu EH, *et al.* (2024): The integrated stress response effector GADD34 is repurposed by neurons to promote stimulus-induced translation. Cell Rep 43:113670.
51. Shrestha P, Ayata P, Herrero-Vidal P, Longo F, Gastone A, LeDoux JE, *et al.* (2020): Cell-type-specific drug-inducible protein synthesis inhibition demonstrates that memory consolidation requires rapid neuronal translation. Nat Neurosci 23:281–292.
52. Blaze J, Akbarian S (2022): The tRNA regulome in neurodevelopmental and neuropsychiatric disease. Mol Psychiatry 27:3204–3213.
53. Edgar RS, Stangherlin A, Nagy AD, Nicoll MP, Efstathiou S, O'Neill JS, Reddy AB (2016): Cell autonomous regulation of herpes and influenza virus infection by the circadian clock. Proc Natl Acad Sci U S A 113:10085–10090.